




Article

Sediment Transport of Coastal Region Using Time-Series Unmanned Aerial Vehicle Spatial Data

Sulki Kim ¹, Sungeol Chang ¹, Sungwon Shin ², Kideok Do ³ and Inho Kim ^{1,*}

¹ Department of Earth and Environmental Engineering, Kangwon National University, Samcheok 25913, Republic of Korea; sg1221@korea.kr (S.K.); sungyeoly@naver.com (S.C.)

² Department of Marine Science and Convergence Engineering, Hanyang University ERICA, Ansan 15588, Republic of Korea; sungwshin@hanyang.ac.kr

³ Department of Ocean Engineering, Korea Maritime & Ocean University, Busan 49112, Republic of Korea; kddo@kmou.ac.kr

* Correspondence: kimih@kangwon.ac.kr; Tel.: +82-33-570-6571

Abstract: Continuous monitoring of the varying topographical characteristics of shorelines is important for effective coastal management. Closed-circuit television (CCTV) cameras are installed to accumulate photographic data on coastal topographical changes. The overall change in the coastal waters can be intuitively understood from the images. However, the amount of three-dimensional (3D) changes that can be grasped is limited. To address this, studies have employed aerial photogrammetry, which is the use of unmanned aerial vehicles (UAVs) to capture aerial pictures, construct 3D models of target areas, and perform analysis through scale-invariant feature transform and structure from motion technologies. Although highly efficient, this technique requires several ground-control points (GCPs), which could corrupt the overall imagery. This study designs real-time kinematics—global navigation satellite system (RTK–GNSS) UAV, which requires few GCPs. To evaluate the positional accuracy of the captured UAV orthographic images and digital surface models (DSMs) used for precise coastal terrain measurements, a virtual reference service survey was performed to determine the vertical errors. The R-squared was 0.985, which is close to 1.0. Short-term and one-year topographic changes before and after a storm were investigated using time-series UAV image data after a coastal maintenance project. Analysis of the coefficient of variation in the beach volume for one year revealed that submerged breakwater reduced erosion during high wave resistance. The submerged breakwater located in the center exhibited variability similar to the opening. Hence, this method is more suitable for periodically monitoring coastal areas.

Keywords: coastal erosion; UAV; submerged breakwater; coastal topography; sediment transport



Citation: Kim, S.; Chang, S.; Shin, S.; Do, K.; Kim, I. Sediment Transport of Coastal Region Using Time-Series Unmanned Aerial Vehicle Spatial Data. *J. Mar. Sci. Eng.* **2023**, *11*, 1313. <https://doi.org/10.3390/jmse11071313>

Academic Editor: Barbara Zanuttigh

Received: 27 May 2023

Revised: 13 June 2023

Accepted: 23 June 2023

Published: 28 June 2023



Copyright: © 2023 by the authors. Licensee MDPI, Basel, Switzerland. This article is an open access article distributed under the terms and conditions of the Creative Commons Attribution (CC BY) license (<https://creativecommons.org/licenses/by/4.0/>).

1. Introduction

Coastal areas are densely populated and conduct bustling economic activities. These areas account for 53% of the world's gross domestic product. However, these areas are at risk of sea-level rise and extreme weather events, such as tropical cyclones, flooding, and other hazards associated with climate change [1].

Erosion and sedimentation occur as sediment is displaced from the beach. As new structures are constructed by a shore, the shoreline changes, and sedimentation destabilizes. Several factors contribute to coastal erosion, including environmental and anthropogenic ones. Coastal erosion caused by these factors can affect the environment and economic activities [2]. Further, the causes of coastal erosion are diverse and depend on the scale. For instance, shoreline retreat (environmental) due to sea-level rise affects large coastal areas relatively slowly, while the construction of coastal structures (anthropogenic) takes years and typically affects smaller coastal areas [3].

Generally, coastal erosion is facilitated by waves. Considering the Korean peninsula as an example, researchers believe that heavy erosion must occur on the east coast of Korea,

where waves are dominant. However, the damage is greater on the west coast, where the tide is high [4]. Particularly, when a typhoon passes the peninsula at high tide, the erosive power of the waves is strengthened, and the erosion damage is severe [5,6]. In particular, the erosion problem of the east coast is more frequently caused by anthropogenic triggers, such as port construction and coastal facility construction, rather than natural events.

Coastal topography significantly changes due to unplanned development and the ensuing coastal damage, which spurs changes in the coastline and the amount of coastal erosion. Beaches are not only important tourist destinations but also valuable natural resources for purifying pollutants and shielding coastal regions from natural disasters. Because coastal topography is constantly changing due to natural and anthropogenic factors, several studies are being conducted to quantitatively analyze and predict changes in beaches and coastlines. Therefore, to effectively manage coastal areas, the topographical changes should be periodically monitored and analyzed. However, due to the low resolution of satellite or aerial images captured at high altitudes, the changes within a few centimeters are difficult to identify. To this end, coastal regions install CCTV cameras that accumulate data on these changes using video images. The overall changes in the coastal waters can be intuitively grasped from these images; however, the degree of change in the three-dimensional (3D) topography that can be perceived is limited. To solve this problem, technology development in connection with various advanced technologies such as satellite and aerial imagery, global navigation satellite system (GNSS), and unmanned aerial vehicles (UAV) has been progressing [7–9]. UAVs that can be deployed rapidly at a relatively low cost have proven highly effective in periodically monitoring coastal topography changes [10,11]. Recently, flight design programs that enable autonomous flight have been developed, allowing to capture aerial images of the desired area. Another study constructed a 3D topographical model through image splicing [12]. This technique is called aerial photogrammetry.

As 3D monitoring technology onboard ultralight UAVs develops, the integration of real-time kinematics—global navigation satellite system (RTK–GNSS), total station, laser imaging detection and ranging (LiDAR), aerial photography, satellite image data, etc., has become possible. Consequently, the limitations of research data can be compensated. Based on the network RTK system, evaluations have demonstrated the possibility of constructing spatial information with a precision of several centimeters by simultaneously surveying the ground-control points (GCPs) [13–15].

UAVs with 3D monitoring shoot aerial pictures and construct 3D models of the target area through the scale-invariant feature transform (SIFT) and structure from motion (SfM) technology to perform topographical analysis. This is more adept than the extant method, and its utilization rate is high [16,17].

In the case of RTK GNSS UAV (DJI Phantom4 RTK) positioning, which corrects for accurate location information, it is generally acceptable to have a distance of approximately 1.0 km between GCPs. Even without GCPs, it is possible to create precise modeling. However, it is advisable to have a minimum of four GCPs placed at the periphery to prevent any potential distortions in the modeling process.

The purpose of this study is to use RTK GNSS UAV to monitor and analyze the coastal erosion in the Cheonjin–Bongpo coastal area, where submerged breakwaters have been constructed as part of coastal maintenance projects over an extended period of time. The study aims to capture the changes in coastal topography before and after a typhoon or swell event and analyze the erosion and deposition processes throughout the entire duration. By utilizing high-resolution images captured by RTK GNSS UAV, this study aims to identify long-term variations in coastal topography and determine the patterns and forms of erosion and deposition. This comprehensive analysis will contribute to a better understanding of the coastal erosion dynamics and provide valuable information for long-term shoreline management and planning.

The remainder of this paper is organized as follows. The study area and wave characteristics are described in Section 2. The aerial survey research method and accuracy

verification results are presented in Section 3. Section 4, the analysis results of topographical changes during the observation period and the short-term changes are presented. Section 5 presents a discussion and conclusion of the study.

2. Site Information

2.1. Study Area

The Cheonjin–Bongpo beach is toward the east of the Korean Peninsula (Figure 1). The seawater there is clean, and the sand size is Coarse and fine, and it is a popular summer resort for both sea fishing and swimming. The beach is adjacent to a port, with small outcrops scattered around and a sandy beach. The coastline is approximately 1.2 km long, with an average beach width of approximately 33 m. It is a northeast-facing, beak-type beach bound by two ports—the Cheonjin Port at the northern end and the Bongpo Port at the Southern (Figure 1). It has a sandy beach, where the median grain size (D_{50}) ranges from approximately 0.70 to 1.13 mm. The spring tide range is 0.18 m, which is a micro-tidal environment. In the target area, severe coastal erosion has been occurring due to the increase in typhoon frequency, climate change, high tides, and coastal infrastructure development. From 2017 to 2019, beach erosion was alleviated by installing submerged breakwater and groin and performing beach nourishment (Figure 2). Four submerged breakwaters and one groin were installed, and detailed specifications for each structure are as follows. Crest height $DL = -0.5$ m; width = 40 m; length = 150 m; and intervals = 80 m. Three submerged breakwaters with a width of 20 m and a length of 50 m, one submerged breakwater with a crest height DL of +1.0 m, and a groin with a length of 40 m were installed. In addition, the submerged breakwater and groin are permeable structures (Tetrapod, TTP).



Figure 1. Location of the study area (Cheonjin–Bongpo Beach).



Figure 2. Before and after coastal maintenance work.

2.2. Wave Characteristics

The current profiler Signature 500 (Nortek) was installed at a depth of approximately DL -25.5 m in the central part of Cheonjin–Bongpo beach to perform short-term wave observations for approximately 10 months (6 April 2020–16 March 2021, Table 1). To analyze the wave characteristics of the site, long-term wave-observation data of Gonghyunjin (Wave Information Network of Korea, WINK), approximately 12 km north of the site, were used (Figure 3). Table 2 provides information on the positions of the two observed points, installation water depth, and observation device.



Figure 3. Wave observation points, W1 and WINK (from Google Earth).

Table 1. Number of observations and duration (W1).

Time	Observation Period	Time	Observation Period
1st	6 April 2020–9 June 2020	2nd	9 June 2020–16 July 2020
3rd	22 July 2020–24 August 2020	4th	24 August 2020–21 October 2020
5th	21 October 2020–26 November 2020	6th	22 January 2021–16 March 2021

Table 2. Wave observation points and water depth.

DIV.	Location	Depth	Observation Device
W1	38°15'38.33" N 128°34'57.92" E	DL (-) 25.5 m	Signature 500 (Nortek)
Gonghyunjin (WINK)	38°21'40.40" N 128°31'41.6" E	DL (-) 32.0 m	AWAC 600 (Nortek)

WINK is a national wave observation system that provides reliable wave data through quality control by collecting wave data of the waters surrounding Korea as observed by the Korea Meteorological Administration, Korea Hydrographic Oceanographic Agency, and the Ministry of Oceans and Fisheries.

The analysis of the significant wave height, peak period, and peak wave direction from the observation data revealed that the incident angle was generally perpendicular to the shoreline. However, it seasonally varies between spring and autumn (ENE-E, low wave energy) and winter (NE-ENE, high wave energy) (Figure 4).

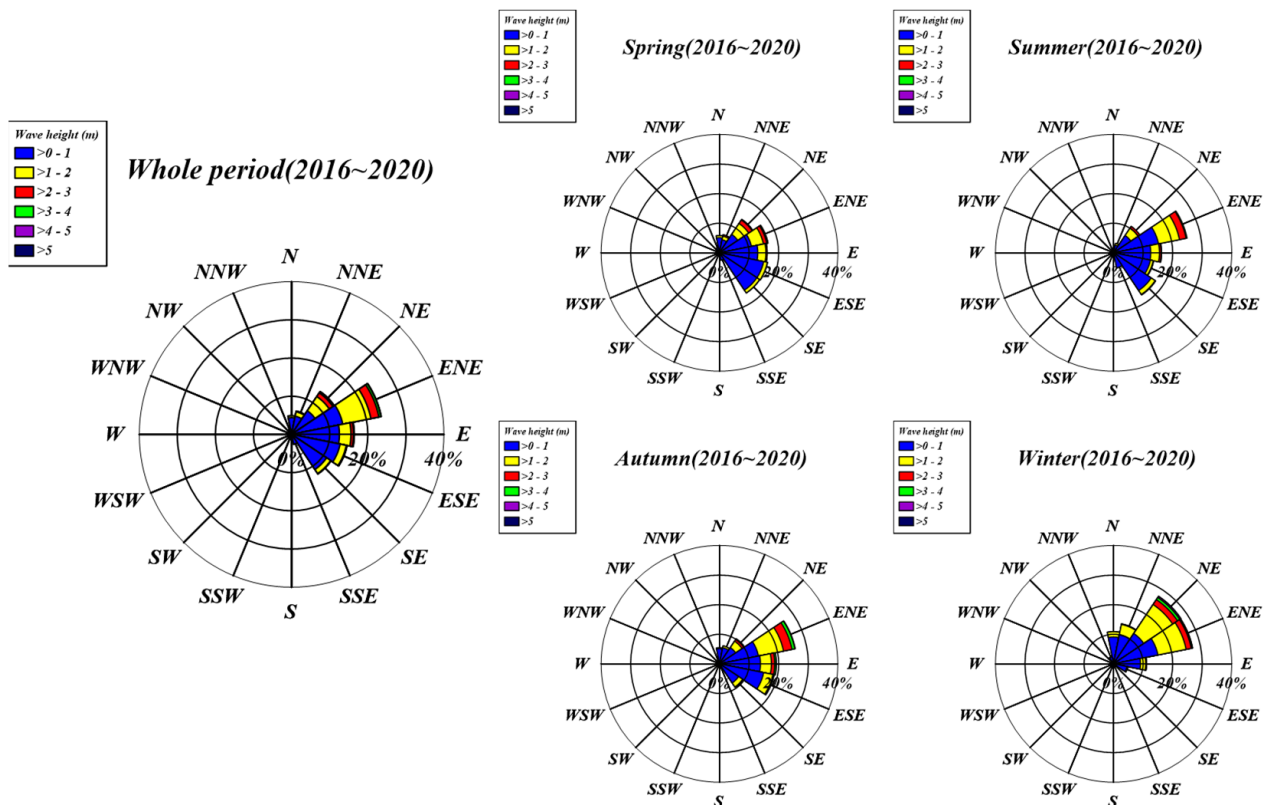


Figure 4. Long-term wave rose (WINK).

During the study period, two typhoons and six swells lashed the study area. Table 3 presents the maximum significant wave height, peak period, peak wave direction, and duration of the significant wave height of 3.0 m or more observed at location W1 during the typhoon and swell events that occurred during the study period. Figure 5 illustrates

the significant wave height, peak period, and time series in the peak direction observed in W1 and WINK, where the blue line represents the UAV observation period. Directional characteristics of waves during typhoon and swell attacks can be divided into two types: waves entering in the vertical direction of the shoreline and those entering from the east. In the cases of Typhoon MAYSAK, HAISHEN, and Swell 2, the wave entered from the east of the coastline (peak direction = 90.42 to 108.46° N), and in the case of the swell, it entered in the vertical direction (peak direction = 58.67 to 75.23° N). As indicated in Table 3 and Figure 5, the maximum significant wave height at the time of the invasion of typhoon MAYSAK was 5.43 m, the peak period was 10.01 s, the duration of the significant wave height over 3.0 m was 4 h. Typhoon HAISHEN lashed the shores at a maximum significant wave height of 5.47 m, a peak period of 11.38 s for a duration of the significant wave height over 3.0 m of 14 h. The maximum significant wave height during the swell invasion was 4.39 m, the peak period was 11.58 s, and the duration of the significant wave height over 3 m was 40 h. A long-time high wave was incident in a direction perpendicular to the shoreline.

Table 3. Typhoons and swell that impacted the study sites during Apr 2020–May 2021, and the characteristics at each storm peak, Hs.

DIV.	Characteristics at Each Storm Peak, Hs				Duration (h) at Hs ≥ 3 m
	Date and Time	Hs (m)	Tp (s)	Dp (°N)	
Swell-1	30 June 2020 12:00	4.08	8.85	58.80	25
Swell-2	24 July 2020 11:00	3.73	7.89	108.46	12
TY-MAYSAY	3 September 2020 09:00	5.43	10.01	101.89	4
TY-HAISHEN	7 September 2020 16:00	5.47	11.38	90.42	14
Swell-3	13 September 2020 13:00	4.39	11.58	59.43	40
Swell-4	29 January 2021 10:00	3.39	11.70	58.67	4
Swell-5	2 March 2021 00:00	5.21	11.43	66.05	28
Swell-6	6 March 2021 13:00	4.97	11.57	75.23	16

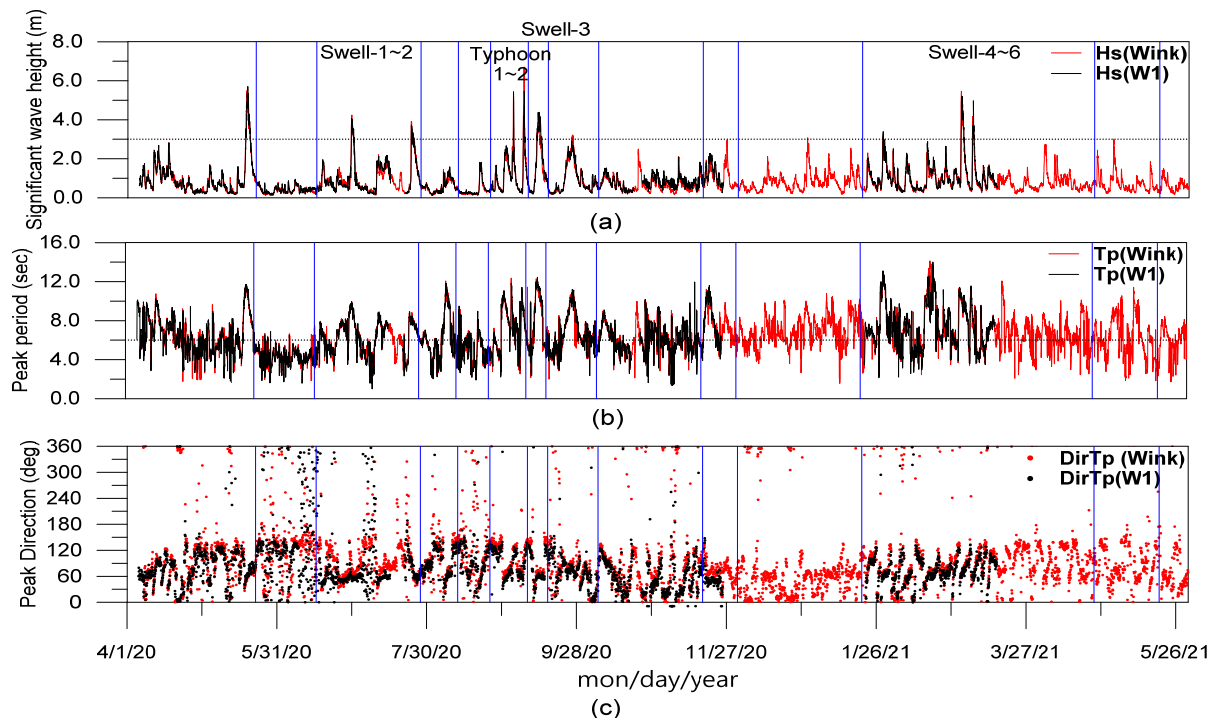


Figure 5. Wave observation time series at W1 (Bongpo, Figure 3) during Apr 2020–May 2021: (a) Significant wave height; (b) peak period; (c) peak direction (based on normal onshore direction); Blue line indicates the date of UAV survey.

3. Method

Aerial surveys were conducted using a UAV to confirm the seasonal and short-term (during typhoons) topographical changes and accurately estimate the erosion and sedimentation at the Cheonjin–Bongpo beach, where the coastal maintenance project was completed. Research methods can be divided into field surveys, e.g., flight planning, GCP survey, aerial photography, and indoor analysis, e.g., SfM-based image processing, accuracy verification of results, and topographic change analysis.

To analyze the short- and long-term topographical changes, 13 aerial surveys were captured in one year (23 May 2020–18 May 2021), including before and after typhoons and during storms. On 28 July 2020, the aerial data were verified during the survey using the network RTK–GPS and the aerial survey results.

3.1. Aerial Survey

As stated earlier, this study employed the DJI Phantom4 RTK (DJI-P4RTK, Shenzhen, Guangong, China), a compact and lightweight UAV with an RGB camera (100 CMOS sensor with 20 M effective pixels, a focal length of 8.8 mm, and an image size of 5472×3648 pixels). The addition of a GNSS antenna receiver module to enable kinematic GNSS on the DJI-P4RTK with centimeter-level accuracy has drawn the interest of researchers to this aircraft in the field of coastal mapping with direct georeferencing. The flight altitude was set to 150 m, the speed to 8 m/s, and the side and forward overlaps to 80%, and the GS RTK application integrated into the remote controller of the UAV was used for flight planning. Approximately 420–460 nadiral images were collected with a mean ground sample distance (GSD) of 4.11 cm/pixel, which was computed considering the flight altitude, sensor dimensions, and focal length. Seven GCPs were selected to orient the captured image, and the position and altitude of the GCPs were surveyed using GNSS (Leica Viva GS16) (Figure 6, Table 4).



Figure 6. Set of ground control point (GCP) locations.

Table 4. Ground control point (GCP) coordinates and elevations.

No.	E	N	Z (DL, m)
GCP1	128°33'41.19"	38°15'33.96"	4.310
GCP2	128°33'36.33"	38°15'35.63"	2.116
GCP3	128°33'34.32"	38°15'33.90"	3.264
GCP4	128°33'43.44"	38°15'19.03"	5.179
GCP5	128°33'44.32"	38°15'18.21"	5.203
GCP6	128°34'02.88"	38°15'08.38"	1.747
GCP7	128°34'03.91"	38°15'09.18"	3.626

3.2. Data Processing

Orthomosaic, DSM, and 3D point clouds were constructed on Pix4D based on the SfM algorithm from the 2D image data of Cheonjin–Bongpo beach acquired using the UAV. Pix4D produces orthomosaic images using the SIFT method and DSM and DTM after creating a high-density point cloud using the SfM method (Figure 7).

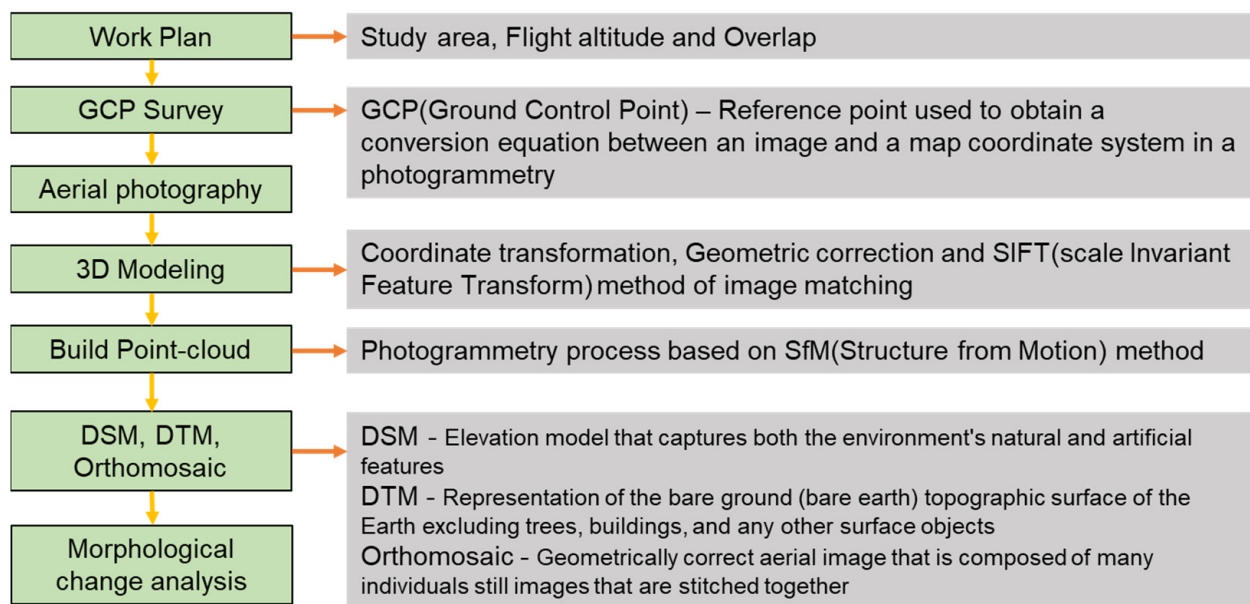


Figure 7. Three-dimensional (3D) modeling flowchart of aerial photogrammetry using UAV.

3.3. Three-Dimensional (3D) Model Accuracy Evaluation

To compare and analyze the time-series image data of beaches and derive quantitative results, the geometrical accuracy of images must be high. A point cloud created for evaluating the accuracy of a 3D model can be evaluated for accuracy in different ways.

To verify the accuracy of UAV survey data, the total beach survey data at 10 m intervals simultaneously observed using the GNSS (Leica Viva GS16), and the aerial survey data corrected using the GCP were compared. The accuracy was also analyzed by comparing the DSM and GNSS survey altitude data (Korean Geoid Model 18) after generating orthogonal grid altitude information at intervals of $dx = dy = 5$ m. Figure 8 presents the results of the accuracy verification of the DTM and GNSS survey results on 25 August 2020. For verification, 1097 pieces of data were used, and the verification result was close to 1.0 with an R^2 of 0.985. Table 5 lists the significant wave height, tidal level, and mean RMS error at the time of observation. During the observation, the maximum significant wave height was 0.81 m, and the tidal level was 0.63 m. As per the analysis, the mean RMS error ranged from 0.40 to 0.72.

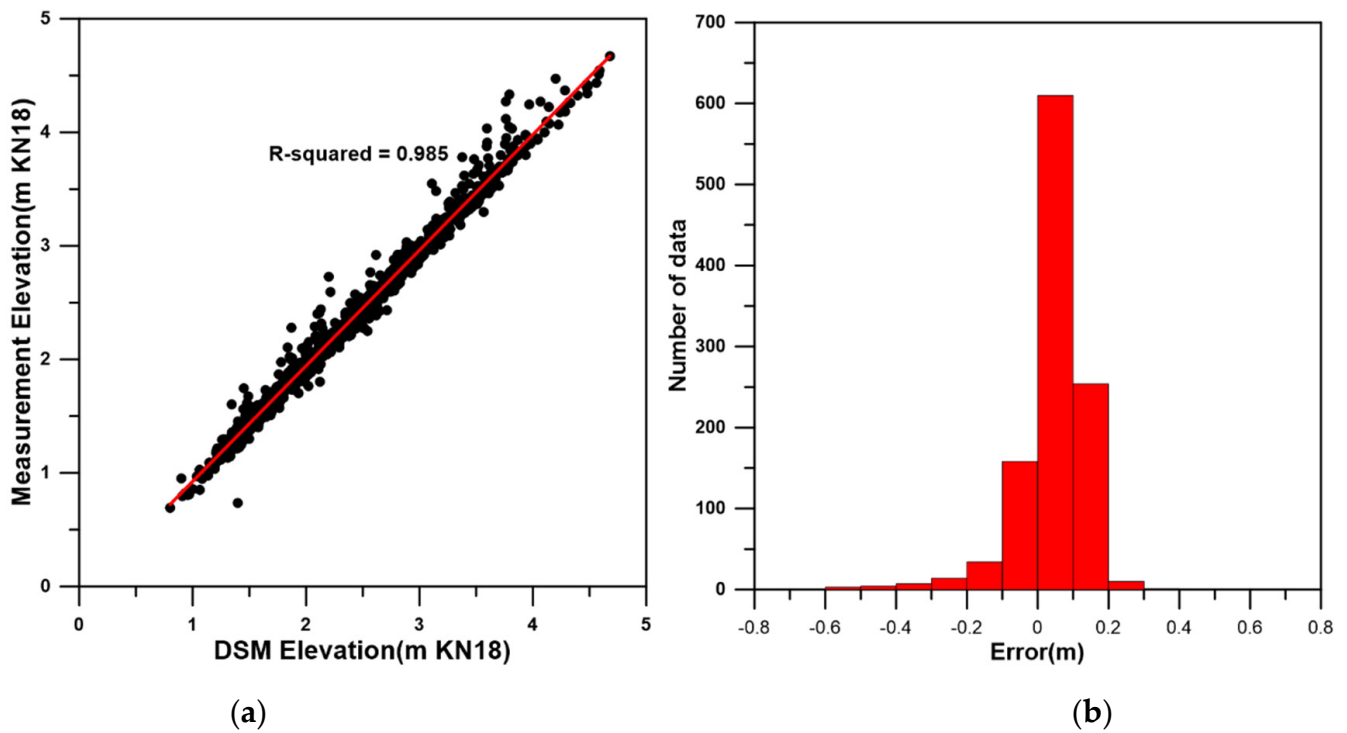


Figure 8. Accuracy analysis: (a) Numerical elevation model accuracy verification result. (b) Error histogram.

Table 5. Mean RMS error, significant wave height, and tide level at the time of observation.

Observation Date (Year/Month/Day/Hour)	Mean RMS Error (m)	Significant Wave Height (m)	Tidal Height (DL, m)
23 May 2020 09–10	0.066	0.81	0.27
16 June 2020 15–16	0.067	0.48	0.38
28 July 2020 08–09	0.056	0.61	0.55
12 August 2020 08–09	0.072	0.37	0.51
25 August 2020 07–08	0.051	0.54	0.63
9 September 2020 07–08	0.052	0.75	0.61
17 September 2020 10–11	0.045	0.45	0.62
7 October 2020 07–08	0.059	0.41	0.37
18 November 2020 11–12	0.049	0.91	0.13
2 December 2020 11–12	0.047	0.54	0.17
21 January 2021 09–10	0.049	0.39	0.17
22 April 2021 11–12	0.061	0.51	0.27
18 May 2021 15–16	0.040	0.56	0.38

According to previous studies, extracting a fixed shoreline by aerial survey is difficult because the shoreline is constantly subjected to wave interference [18]. In this study, an elevation of 1.0 m or higher was analyzed considering the waves and tides at the time of observation.

4. Results

4.1. Long-Term Topographical Changes

To measure the topographical change, the model used images captured 13 times a year. The width of the beach was set at 50 m intervals, and the area considering the influence of the coastal structures was set as illustrated in Figure 9. To analyze the variability of the beach’s physical dimensions, the coefficient of variation ($CV = \frac{s}{\bar{x}}$), which is the standard deviation divided by the average value, was used. The CV is expressed as a number that indicates the degree of spread about the sample mean. As the area and volume changes

exhibit a major difference in the scale according to the size of the area, a normalization process was required to reflect them on the same scale. In general, the most popular normalization methods are min/max and z-score. Min/max normalization does not stably handle outliers, despite all features having the same scale. Therefore, in this study, analysis was performed using the z-score normalization method, which stably handles outliers.

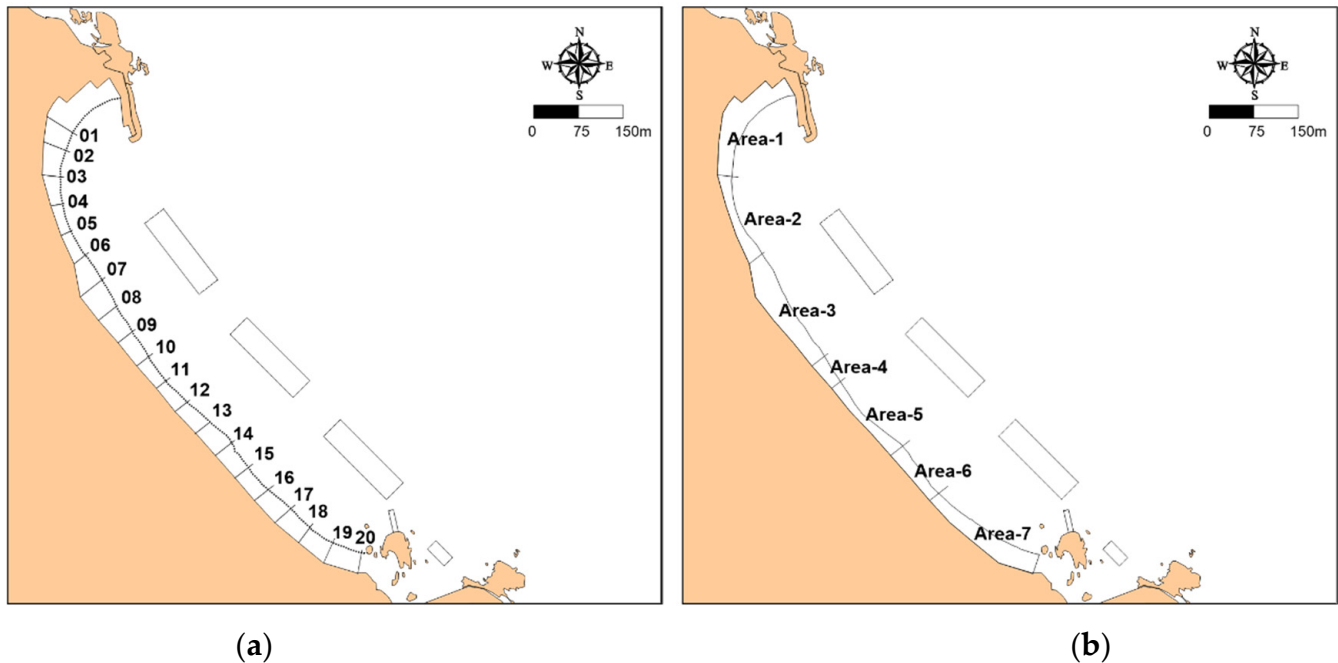


Figure 9. Analysis criteria and areas: (a) beach width baseline; (b) beach area and volume zones.

The changes in the beach width by baseline and z-score-normalized time series of change in the beach volume by zone are presented in Figure 10. Looking at the short-term changes in topography in the beach width by baseline and area before the typhoon passage, the baseline for beach widths 1 to 4 (areas 1 and 2) and 12 to 16 (area 5) decreased. However, after the typhoon passage, both the area and beach width increased. But after the Swell 3 passage, the beach width and area decreased. These changes in the topography are highly correlated with wave energy, and during the typhoon passage, the duration of significant wave heights exceeding 3.0 m lasted for 2 to 14 h. However, during Swell 3 passage, the duration extended to 40 h, indicating a significant difference in the duration.

The CV of beach volume is presented in Table 6. The CV and beach width, which is the rear area of the northern breakwater and submerged breakwater (1, 3, and 7 zones), is small, and between the submerged breakwaters (2, 4, and 6 zones) is a common phenomenon. However, the changing pattern of Area 5, which is the rear of the central part of the underwater breakwater, is significantly different from the rear area of other structures. We believe this phenomenon occurs due to the difference in the transmission coefficient of the submerged breakwater. A detailed investigation of the parameters of the installed latent material, such as crest height, width, and transmission coefficient measurement, of the relevant structure, is required. The coefficient appeared to decrease as the wave period and incident wave direction angle increased [19].

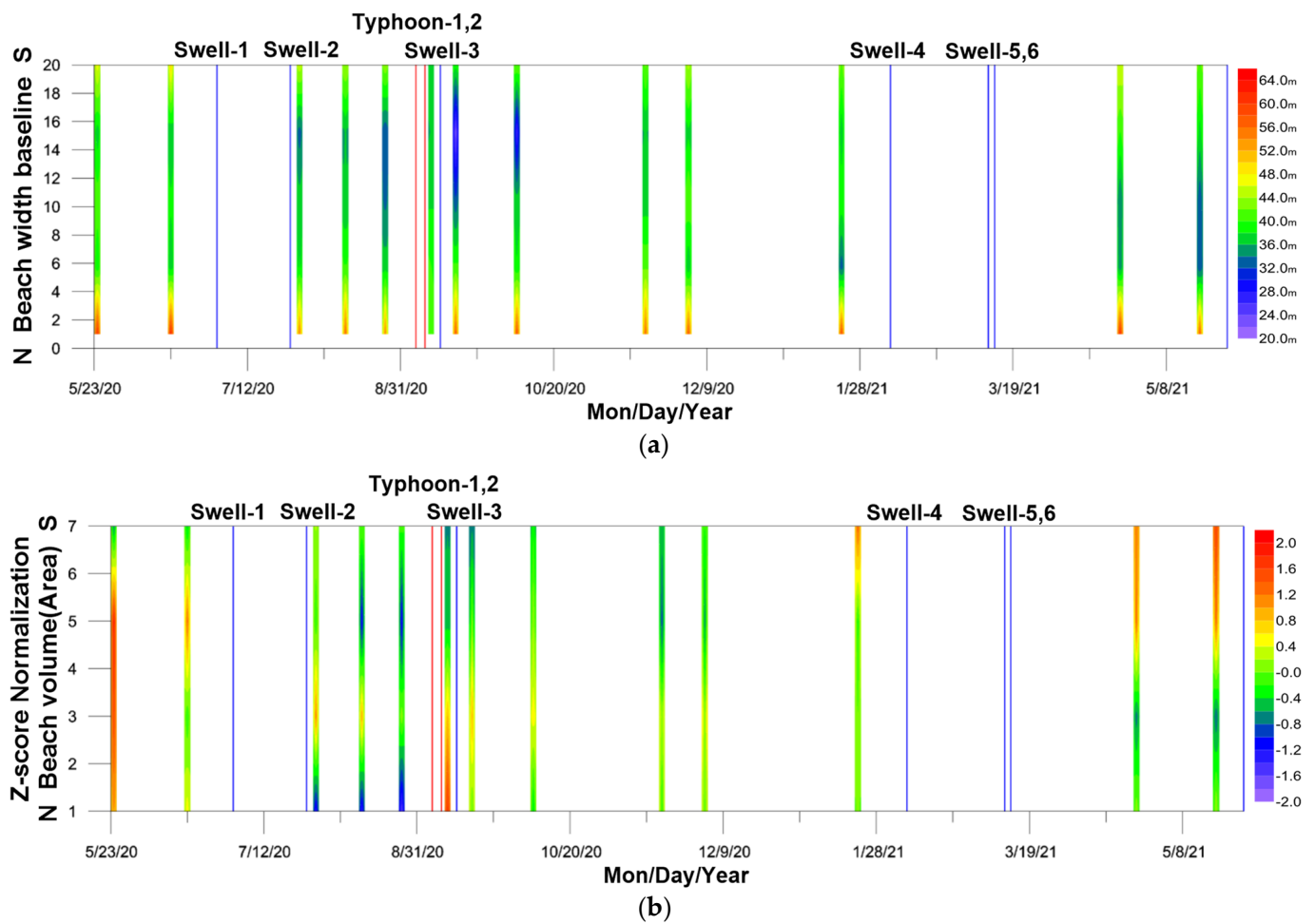


Figure 10. Beach-volume and beach-width time series: (a) Beach width. (b) Beach volume for each zone with z-score normalization. Blue line indicates swell and red line indicates typhoon.

Table 6. Average beach volume, standard deviation, and coefficient of variation by area.

DIV.	Area-1	Area-2	Area-3	Area-4	Area-5	Area-6	Area-7
	BW		SBW		SBW		SBW
Average volume (m ³)	14,796	7904	20,028	2910	8667	5180	16,585
Standard deviation	1246	1338	1044	465	1313	1201	1071
Coefficient of variation	0.08	0.17	0.05	0.16	0.15	0.21	0.06

4.2. Short-Term Topography Change

The short-term topographic changes were analyzed using the results observed within two weeks before and after the typhoon and swell. Figure 11 illustrates the variations in beach height, beach width, significant wave height, peak period, peak wave direction, main wave direction, and wave direction with a significant wave height of 3 m or more before and after the typhoon and swell attacks. Table 7 presents the values obtained by volume for each area displayed in Figure 9b.

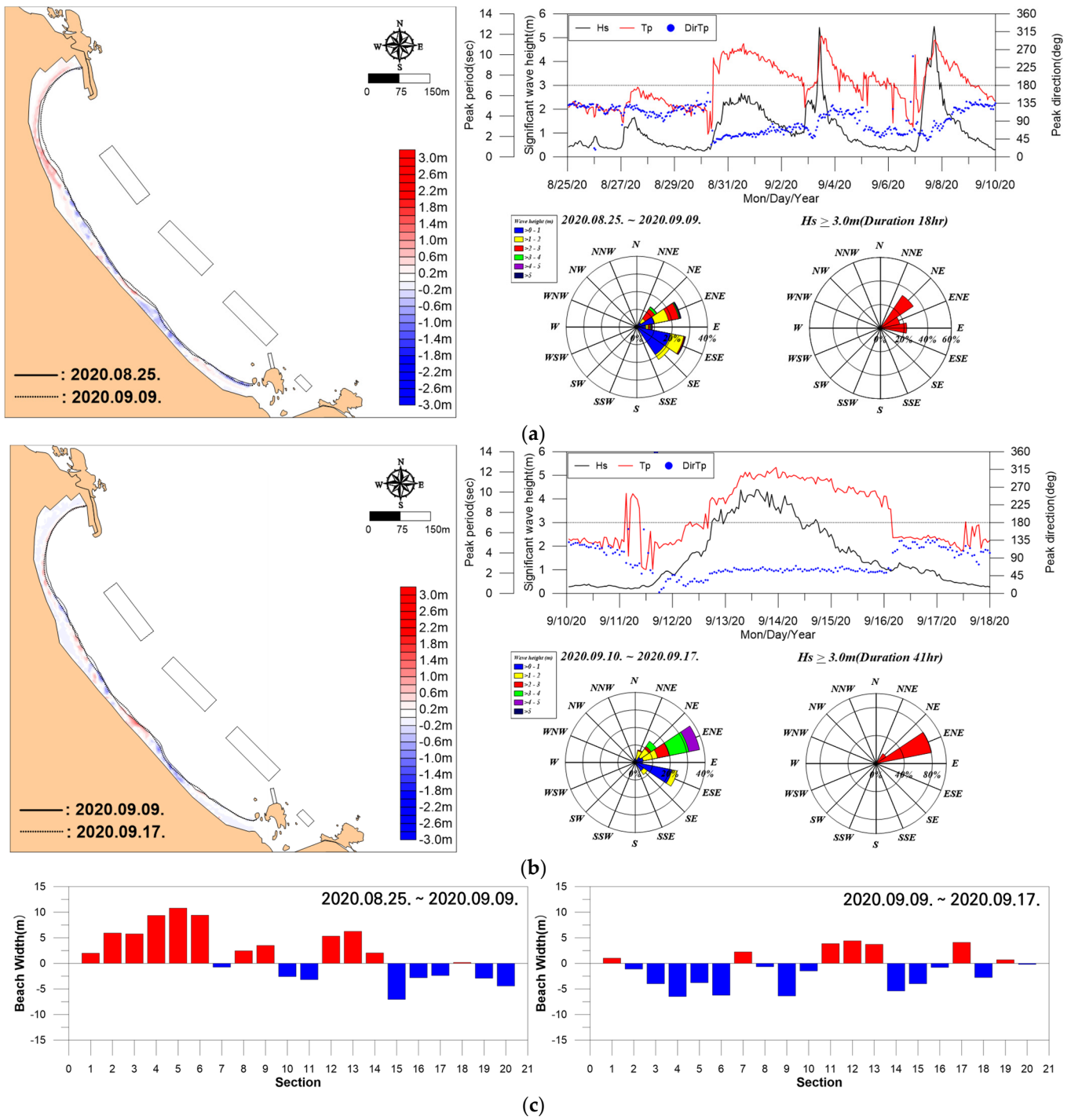


Figure 11. Short-term topographical change (changes in beach elevation, red; accumulation, blue; erosion) and significant wave height, peak period, and peak wave direction during storms: (a) during typhoon; (b) swell; and (c) change in beach width.

Table 7. Area beach volume changes by observation date.

Date	Area-1	Area-2	Area-3	Area-4	Area-5	Area-6	Area-7
	BW		SBW		SBW		SBW
25 August 2020	12,763	6730	20,004	3336	6840	5573	16,178
9 September 2020	17,412	9704	20,866	2498	7838	4347	15,519
17 September 2020	14,982	9544	20,888	2363	8656	3560	15,477

Figure 11a depicts the topographical changes and wave time-series data before and after the two typhoons in early September 2020. The maximum significant wave height was approximately 5.5 m, the peak period was 11.4 s, and the peak wave direction was E. A significant wave height of 3 m or more was observed for a duration of approximately 18 h. The topographical changes during the typhoon attack period reveal that sedimentation was dominant on the north coast (volumes of Area-1 and Area-2 increased), and erosion prevailed on the south (volumes of Area-4, Area-6, and Area-7 decreased). In addition, it indicated that sediment or erosion was relatively small in the rear end of the submerged breakwater than at the opening (volumes of Area-3 and Area-5 increase). Figure 11c represents the changes in beach width by baseline. During the typhoon passage, there was an increase in beach width in the northern section and a decrease in the southern section. However, during the swell passage, with some exceptions in certain sections behind the central submerged breakwater, most of the beach widths decreased.

After the typhoon, swell waves occurred, and the maximum significant wave height was approximately 4.4 m, the peak period was 11.6 s, and the peak wave direction was ENE series. A significant wave height of 3 m or more was observed for approximately 41 h, i.e., the swell lasted for a long time (Figure 11b). Unlike the topographical change during typhoons, erosion of the beach occurred mainly on the northern side. The rear of the submerged breakwater and the opening section exhibited similar tendencies. When the typhoon lashed the peninsula, the storm lasted for a short time, and the wave moved from NE to SE. However, during the swell, the waves continued for a longer duration in the same direction. Owing to the submerged breakwater installation, no significant change occurred in the topography during high-tide storms.

5. Discussion and Conclusions

Measuring changes in the elevation or shoreline is important for studies on coastal topographical changes. Recently, surveying techniques using UAVs have come under the spotlight owing to their cost effectiveness and survey quality [20]. A topographical model can be constructed by rapidly observing a relatively large area and accurately investigating the area of interest before or after high waves or on a specific day. This approach is widely used in various fields, including glacial topography detection [21], river topographical change [22], and slope topographical change due to landslides [23]. Particularly, surveying technology using UAVs is useful for tracking changes in beach topography [24,25]. To detect only topographical changes only at the coastline, the coastline can be extracted from the orthographic image acquired by the drone and analyzed swiftly with techniques such as a digital shoreline analysis system. In addition, numerical elevation models can be constructed to detect changes in volume or area with high accuracy.

In this study, a precise numerical elevation model was established by performing network RTK-UAV-based surveillance of the coast of the Cheonjin-Bongpo beach, where a coastal maintenance project was completed recently. The short-term and one-year topographical changes before and after storms were investigated using the time-series UAV image data constructed using the proposed method. Short-term changes in topography were examined by measuring before and after the passage of typhoons or swells. In this study, wave observation data, along with changes in volume and beach width by section, were utilized. Generally, the most significant factors influencing short-term topographic changes are wave direction and the duration of high-energy wave events. However, based on the observation results of wave direction for significant wave heights exceeding 3.0 m in the study area, it is inferred that there would not be significant differences in wave direction in the shallow offshore zone due to refraction caused by water depth. For this reason, it is determined that the duration of high-energy waves rather than the magnitude of wave height is the primary factor influencing major topographic changes in the study area. An analysis of the CV of the beach volume for one year revealed that submerged breakwater reduced erosion during high wave resistance. The CV for the areas behind submerged breakwaters 1 and 3 is 0.05 and 0.06, respectively. However, for submerged breakwater 2,

the CV is 0.15, which is similar to the CV ranging from 0.16 to 0.21 observed for the opening sections of submerged breakwaters 2, 4, and 6. In turn, it reduces the energy caused by the breaking waves when high waves enter the coast; however, detailed investigations are required for structures with increased wave height or crown elevation of submerged breakwater owing to the shoaling effect in deep-water waves. Although the duration of this study was only one year, the aerial surveys along the coastline could rapidly and accurately construct spatial information compared to the extant aerial photogrammetry method. Hence, the proposed 3D topographical modeling using time-series UAV images is suitable for the periodic monitoring of coastal areas.

A limitation of this study is that although UAV-based beach monitoring is an efficient method in terms of time and input, it does not have sufficient tools to analyze beach sediments and determine the foreshore slope in the wave-breaking zone. If the particle size of sediments can be analyzed and the foreshore slope can be measured in the future, the acquired data could be used to explain the topographical changes of beaches.

Author Contributions: Conceptualization, I.K., S.S. and K.D.; methodology, S.K. and K.D.; software, S.K. and S.C.; validation, S.K. and S.C.; formal analysis, S.K.; investigation, S.K., S.C. and K.D.; resources, I.K.; data curation, I.K.; writing—original draft preparation, S.K., S.C., K.D. and S.S.; writing—review and editing, S.K., S.C., K.D., S.S. and I.K.; visualization, S.K.; supervision, S.S. and I.K.; project administration, K.D. and S.S.; funding acquisition, I.K. All authors have read and agreed to the published version of the manuscript.

Funding: These are the research results of the 2017 Kangwon National University Basic Research Fund Support Project (620170060).

Institutional Review Board Statement: Not applicable.

Informed Consent Statement: Not applicable.

Data Availability Statement: Not applicable.

Conflicts of Interest: The authors declare no conflict of interest.

References

1. UN-Habitat. *Planning Sustainable Cities Global Report on Human Settlements 2009*; UN-Habitat: Nairobi, Kenya, 2016.
2. Saadon, M.S.I.; Ab Wahida, N.S.; Othman, M.R.; Nor, D.A.M.; Mokhtar, F.S.; Nordin, N.; Kowang, T.O.; Nordin, L. An evaluation of the impact of coastal erosion to the environment and economic activities at Mengabang Telipot, Terengganu. *J. Crit. Rev.* **2020**, *7*, 1132–1136.
3. Komar, P.D. Coastal erosion—Underlying factors and human impacts. *Shore Beach* **2000**, *68*, 3–16.
4. Kwon, H.J. Coastal erosion of western coast of Korea. *Bull. Coll. Educ.* **1993**, *18*, 137–155. (In Korean)
5. Yoon, J.J.; Jun, K.C.; Shim, J.S.; Park, K.S. Estimation of maximum typhoon intensity considering climate change scenarios and simulation of corresponding storm surge. *J. Korean Soc. Mar. Environ. Energy* **2012**, *15*, 292–301. (In Korean) [[CrossRef](#)]
6. Kang, T.S.; Oh, H.M.; Lee, H.M.; Eum, H.S. Storm surge vulnerability assessment due to typhoon attack on coastal area in Korea. *Korean Soc. Mar. Environ. Saf.* **2015**, *21*, 608–616. (In Korean) [[CrossRef](#)]
7. Wojciech, G.; Wojciech, M.; Pawel, C. Comparison of low-altitude UAV photogrammetry with terrestrial laser scanning as data-source methods for terrain covered in low vegetation. *ISPRS J. Photogramm. Remote Sens.* **2017**, *126*, 168–179.
8. Artur, W.; Przemyslaw, K.; Bartosz, M.; Izabela, P. The use of TLS and UAV methods for measurement of the repose angle of granular materials in terrain conditions. *Measurement* **2019**, *146*, 780–791.
9. Shikai, S.; Yu, P.; Chenglong, H.; Yun, D. Efficient path planning for UAV formation via comprehensively improved particle swarm optimization. *ISA Trans.* **2020**, *97*, 415–430.
10. Dalamagkidis, K.; Valavanis, K.P.; Piegł, L.A. On unmanned aircraft systems issues, challenges and operational restrictions preventing integration into the National Airspace System. *Prog. Aerosp. Sci.* **2008**, *44*, 503–519. [[CrossRef](#)]
11. Chiabrande, F.; Nex, F.; Piatti, D.; Rinaudo, F. UAV and PRV systems for photogrammetric surveys in archaeological areas: Two tests in the Piedmont region. *J. Archaeol. Sci.* **2011**, *38*, 697–710. [[CrossRef](#)]
12. Rhee, S.A.; Kim, T.J.; Kim, J.I.; Kim, M.C.; Chang, H.J. DSM generation and accuracy analysis from UAV images on river-side facilities. *Korean J. Remote Sens.* **2015**, *31*, 183–191. (In Korean) [[CrossRef](#)]
13. Jung, S.H.; Lim, H.M.; Lee, J.K. Acquisition of 3D spatial information using UAV photogrammetric method. *J. Korean Soc. Surv. Geod. Photogramm. Cartogr.* **2010**, *28*, 161–168. (In Korean)
14. Kim, D.I.; Song, Y.S.; Kim, C.W. A study on the application of UAV for Korean land monitoring. *J. Korean Soc. Surv. Geod. Photogramm. Cartogr.* **2014**, *32*, 29–38. (In Korean) [[CrossRef](#)]

15. Lim, S.B.; Seo, C.W.; Yun, H.C. Digital map updates with UAV photogrammetric method. *J. Korean Soc. Surv. Geod. Photogramm. Cartogr.* **2015**, *33*, 397–405. (In Korean) [[CrossRef](#)]
16. Long, N.; Millescamp, B.; Guillot, B.; Pouget, F.; Bertin, X. Monitoring the topography of a dynamic tidal inlet using UAV imagery. *Remote Sens.* **2016**, *8*, 387. [[CrossRef](#)]
17. Turner, I.L.; Harley, M.D.; Drummond, C.D. UAVs for coastal surveying. *Coast. Eng.* **2016**, *114*, 19–24. [[CrossRef](#)]
18. Choi, K.; Kong, H.; Jung, S.; Park, S.; Lee, S. Coastal change detected using drone-based mapping in Hashidong beach, Gangneung, South Korea. *J. Korean Geomorphol. Assoc.* **2016**, *23*, 101–112. (In Korean) [[CrossRef](#)]
19. Jeong, J.H.; Kim, J.H.; Lee, J.L. Analysis of wave transmission characteristics on the TTP submerged breakwater using a parabolic-type linear wave deformation model. *J. Ocean Eng. Technol.* **2021**, *35*, 82–90. [[CrossRef](#)]
20. Cook, K.L. An evaluation of the effectiveness of low-cost UAVs and structure from motion for geomorphic change detection. *Geomorphology* **2017**, *278*, 195–208. [[CrossRef](#)]
21. Clark, A.; Moorman, B.; Whalen, D.; Fraser, P. Arctic coastal erosion: UAV-SfM data collection strategies for planimetric and volumetric measurements. *Arct. Sci.* **2021**, *7*, 605–633. [[CrossRef](#)]
22. Miřijovský, J.; Langhammer, J. Multitemporal monitoring of the morphodynamics of a mid-mountain stream using UAS photogrammetry. *Remote Sens.* **2015**, *7*, 8586–8609. [[CrossRef](#)]
23. Fiorucci, F.; Giordan, D.; Dutto, F.; Rossi, M.; Guzzetti, F. Geomorphological mapping of shallow landslides using UAVs. *EGU Gen. Assem. Conf. Abstr.* **2015**, *17*, 14993.
24. Casella, E.; Rovere, A.; Pedroncini, A.; Stark, C.P.; Casella, M.; Ferrari, M.; Firpo, M. Drones as tools for monitoring beach topography changes in the Ligurian Sea (NW Mediterranean). *Geo-Mar. Lett.* **2016**, *36*, 151–163. [[CrossRef](#)]
25. Pérez-Alberti, A.; Trenhaile, A.S. An initial evaluation of drone-based monitoring of boulder beaches in Galicia, north-western Spain. *Earth Surf. Process. Landf.* **2015**, *40*, 105–111. [[CrossRef](#)]

Disclaimer/Publisher's Note: The statements, opinions and data contained in all publications are solely those of the individual author(s) and contributor(s) and not of MDPI and/or the editor(s). MDPI and/or the editor(s) disclaim responsibility for any injury to people or property resulting from any ideas, methods, instructions or products referred to in the content.

Reproduced with permission of copyright owner. Further reproduction prohibited without permission.